NAVAL POSTGRADUATE SCHOOL
Monterey, California

THESIS

APPLICATIONS OF INFRARED THERMOGRAPHY IN CONVECTIVE HEAT TRANSFER

by

Timothy M. Spence

March 1986

Thesis Advisor: R.H. Nunn

REPORT DOCUMENTATION PAGE

REPORT SECURITY CLASSIFICATION Unclassified	1b. RESTRICTIVE MARKINGS
. SECURITY CLASSIFICATION AUTHORITY	3 DISTRIBUTION / AVAILABILITY OF REPORT Approved for public release; distribution is unlimited
. DECLASSIFICATION / DOWNGRADING SCHEDULE	
PERFORMING ORGANIZATION REPORT NUMBER(S)	5. MONITORING ORGANIZATION REPORT NUMBER(S)
. NAME OF PERFORMING ORGANIZATION aval Postgraduate School	6b. OFFICE SYMBOL (If applicable) Code 69
7a. NAME OF MONITORING ORGANIZATION Naval Postgraduate School	
. ADDRESS (City, State, and ZIP Code) onterey, California 93943-5000	7b. ADDRESS (City, State, and ZIP Code) Monterey, California 93943-5000
. NAME OF FUNDING / SPONSORING ORGANIZATION	8b. OFFICE SYMBOL (If applicable)
9. PROCUREMENT INSTRUMENT IDENTIFICATION NUMBER	
. ADDRESS (City, State, and ZIP Code)	10 SOURCE OF FUNDING NUMBERS

PROGRAM ELEMENT NO	PROJECT NO	TASK NO	WORK UNIT ACCESSION NO

TITLE (Include Security Classification)
PPLICATIONS OF INFRARED THERMOGRAPHY IN CONVECTIVE HEAT TRANSFER

PERSONAL AUTHOR(S)
pence, Timothy M.

a TYPE OF REPORT	13b TIME COVERED	14 DATE OF REPORT (Year, Month, Day)	15 PAGE COUNT
laster's Thesis	FROM _____ TO _____	1986, March	69

SUPPLEMENTARY NOTATION

COSATI CODES		
FIELD	GROUP	SUB-GROUP

18 SUBJECT TERMS (Continue on reverse if necessary and identify by block number)
Infrared Thermography; TVC Convective Heat Transfer

ABSTRACT (Continue on reverse if necessary and identify by block number)

A full-scale model of a double-wedge, simulating a jet vane used in guided missile thrust vector control (TVC), was constructed for subsonic wind tunnel testing to evaluate the feasibility of utilizing a thermal imaging (infrared) system vice thermocouples to determine a surface heat transfer coefficient. The model was preheated, then allowed to cool via forced convection to ambient conditions. Surface temperature readings were taken using thermocouples and a thermal imaging system during the cooldown process. These readings were then reduced to solve for a heat transfer coefficient (h), using Newton's Law of Cooling. The results were compared with the theoretical solution for a flat plate and with the results obtained by testing an actual TVC vane configuration under the identical flow conditions.

0 DISTRIBUTION / AVAILABILITY OF ABSTRACT ☒ UNCLASSIFIED/UNLIMITED ☐ SAME AS RPT ☐ DTIC USERS	21. ABSTRACT SECURITY CLASSIFICATION Unclassified
2a NAME OF RESPONSIBLE INDIVIDUAL Prof. Robert H. Nunn	22b TELEPHONE (Include Area Code) (408) 646-2365 / 22c. OFFICE SYMBOL Code 69Nn

Approved for public release; distribution is unlimited.

Applications of Infrared Thermography in Convective Heat Transfer

by

Timothy M. Spence
Lieutenant Commander, United States Navy
B.S., University of Mississippi, 1976

Submitted in partial fulfillment of the
requirements for the degree of

MASTER OF SCIENCE IN MECHANICAL ENGINEERING

from the

NAVAL POSTGRADUATE SCHOOL
March 1986

ABSTRACT

A full-scale model of a double-wedge, simulating a jet vane used in guided missile thrust vector control (TVC), was constructed for subsonic wind tunnel testing to evaluate the feasibility of utilizing a thermal imaging (infrared) system vice thermocouples to determine a surface heat transfer coefficient. The model was preheated, then allowed to cool via forced convection to ambient conditions. Surface temperature readings were taken using thermocouples and a thermal imaging system during the cooldown process. These readings were then reduced to solve for a heat transfer coefficient (h), using Newton's Law of Cooling. The results were compared with the theoretical solution for a flat plate and with the results obtained by testing an actual TVC vane configuration under the identical flow conditions.

TABLE OF CONTENTS

LIST OF TABLES

LIST OF FIGURES

ACKNOWLEDGEMENT

The author wishes to acknowledge the contributions of the following individuals, whose assistance was invaluable and greatly appreciated:

Mr. James Scholfield, Department of Mechanical Engineering

Mr. John Moulton, Department of Mechanical Engineering

I. INTRODUCTION

A. BACKGROUND

The use of thrust vector control (TVC) in future cruise missile guidance and control systems is presently being investigated. Removing external aerodynamic steering surfaces (fins) would allow installation of a single weapon configuration in multiple platforms with little or no restructuring of each platform's unique launch capabilities, thereby reducing design, development, and construction costs. In addition, the maneuvering envelopes required of present and future missiles may contain regions in which external aerodynamic surfaces are inadequate for control purposes.

The incorporation of TVC systems for missile steering requires the design of jet vanes, or other deflection devices, that are mounted in the rocket exhaust flow. Such devices can be rotated to various angles of attack in order to redirect the flow, thus maneuvering the missile in the desired direction. The vanes must be made to withstand severe steady and transient thermal loads, shock wave impingement, and erosion from motor exhaust particulates during extended use.

One of the first steps in the design of such a vane is to develop a model of the thermal environment to which the vane will be subjected. This includes the determination of surface heat transfer coefficients for particular vane configurations under forced convection conditions.

The following discussion concerns the development of experimental methods to determine a heat transfer coefficient on a heated surface in subsonic flow. Utilizing state-of-the-art infrared technology, in place of thermocouples, to determine surface temperature gradients as a body is heated (or cooled, as in this case) would reduce the time and effort required to develop instrumented models. The method also has the potential to reduce or eliminate the need for elaborate data acquisition systems, while maintaining an accuracy that is at least as good as that obtained from conventional methods. Finally, the methods described here provide a global as well as local view of surface heat transfer. Thus it is possible to detect and analyze regions of particular interest that might otherwise go unnoticed in the data produced by point temperature measurements.

B. OBJECTIVES

The objectives of this study are to:

1) Design a typical TVC model instrumented for surface temperature measurement using both thermocouples and thermal imaging technology.

2) Record surface temperatures of the model in a subsonic wind tunnel environment.

3) Compare the results from both measurement techniques in calculating the heat transfer coefficient, using Newton's Law of Cooling, and correlating the results with the theoretical solution for a flat plate under identical flow conditions.

4) Utilize the thermal imaging technique to analyze the surface temperature map of an actual TVC vane configuration.

5) Present conclusions and recommendations for future applications in this area.

II. MODEL DESIGN AND CONSTRUCTION

A. MODEL DESIGN

A double-wedge design was chosen for this experiment for several reasons, including ease of construction, similarity to typical TVC configurations used in previous research, and sufficient similarity to a flat plate to allow interpretation of results. A drawing of the wedge is included as Figure 1.

The dimensions of the model were chosen to reflect essentially full-scale, but constrained by the necessity of having a Biot number less than 0.1. This constraint is mandated by the use of the lumped-heat capacitance analogy in this experiment to determine the heat transfer coefficient [Ref. 1]. This method of analysis assumes that the internal resistance of the body is negligible compared to the external resistance and, therefore, a uniform temperature distribution exists throughout the model. By ensuring that the model has a Biot number less than 0.1, this analytical method will produce reliable results.

The convection heat loss from the heated model is assumed to equal the decrease in its internal energy. Thus, the energy balance expressing the rate of heat transfer, q, is:

$$q = hA(T - T_\infty) = - c \rho V \frac{dT}{dt}$$

where:

$h \equiv$ heat transfer coefficient, BTU/hr-ft^2-°F

$A \equiv$ surface area, ft^2

$T \equiv$ model temperature at time t, °F

$T_\infty \equiv$ free stream temperature, °F

$c \equiv$ heat capacity of model material, BTU/lbm-°F

$V \equiv$ model volume, ft^3

$k \equiv$ thermal conductivity, BTU/hr-ft-°F

$\rho \equiv$ density, lbm/ft^3.

Given the initial condition of $T = T_o$ at time $t = 0$, the solution to the differential equation becomes:

$$\frac{T - T_\infty}{T_o - T_\infty} = \exp - (Bi \times Fo)$$

where:

Bi Biot number $= \frac{hV}{kA}$

Fo Fourier number $= \frac{k}{\rho c}\left(\frac{A}{V}\right)^2 t$

B. CONSTRUCTION

Copper was chosen as the model material due to its excellent thermal conductivity (k = 230 BTU/hr-ft-°F) and reasonably good machinability. With the dimensions as shown in Figure 1, giving V/A = 0.01297, the surface heat transfer coefficient could theoretically rise to well over h = 1400 BTU/hr-ft^2-°F

before the restriction on Biot number would be violated. As the expected heat transfer coefficient was less than 60, these design decisions ensured excellent accuracy in applying the method.

The copper wedge was instrumented with copper-constantin (type T) thermocouples, 30 gauge. The thermocouples were placed as shown in Figure 1, with one of the thermocouples embedded at depth of 0.30 inches to detect any distinguishable temperature difference between the surface and the interior. As can be seen in the subsequent tables and graphs, the assumption of Newtonian cooling proved to be accurate. The wedge was also covered with a thin coat of flat black paint to increase the emissivity of the surface to a minimum of 0.95 [Ref. 1] in order to enhance the thermal image detection of the infrared system.

The thermocouples were attached to a dual-channel strip chart recorder, and to a digital temperature sensor. The digital readout was used to obtain reference values of wedge temperature during heatup, and free stream temperatures during testing. All instruments and thermocouples were calibrated from 32°F to 150°F using the Department of Mechanical Engineering calibration facility.

The wedge was then mounted on two aluminum stanchions, attached to the plexiglass insert in the floor of the wind tunnel test section. Within the plexiglass, a six-inch diameter hole was cut for insertion of the infrared-transparent

window through which the thermal imaging system could view the wedge surface. This arrangement is shown in Figure 2. Plexiglass sidewalls were added to form a thermal barrier to attempt to negate any spanwise heat transfer from the wedge sides, and to form a channel for uniform air flow past the wedge. The model was heated by using an electric pad, capable of raising temperatures from ambient to approximately 140°F within a thirty minute time frame.

III. THERMAL IMAGING SYSTEM

A. DESCRIPTION

The thermal imaging system used in this procedure is a Probeye Thermal Video System, Series 4300, manufactured by Hughes Aircraft Company [Ref. 2]. This system provides real-time temperature maps of objects through 16 color bands displayed on a color monitor. The temperature range of the system is from -4°F to 536°F (-40°C to +280°C). Each color on the scale can represent temperature sensitivities from 0.5 to 36°F (0.5 to 20°C), depending upon the desired overall temperature range. Emissivity adjustments can be made from 0.0 to 1.0 in increments of 0.01, in the spectral wavelength band of 2.0 to 5.6 μmeters. The unit includes a movable cursor which can be placed at any location on the viewed surface, giving a digital readout of the temperature at that location, and a real time clock/calendar precise to 0.1 seconds for determining time-variant conditions.

The use of this imaging system also required the use of an infrared optic window for viewing the model while maintaining tunnel integrity. A six-inch diameter, two millimeter thick window fabricated from magnesium fluoride was obtained from Eastman Kodak Company. This type of material, tradename IRTRAN 1, was chosen to match the optical wavelength characteristics of the imaging system. As manufactured, the window

allowed over 95% transmittance in the 2.0 to 5.8 μmeter range, while capable of withstanding pressure differentials of 1 atmosphere at 25°C, with a factor of safety of four [Ref. 3].

IV. EXPERIMENTAL PROCEDURE

A. WIND TUNNEL TESTING

The model assembly, as shown in Figure 2, was installed in the test section of the subsonic wind tunnel. This wind tunnel is a pull-down system capable of producing test section free stream velocities of up to 335 feet/second by means of a variable speed fan located at the tunnel exit. The free-stream turbulence level of the tunnel (0.2%-0.5%) was deemed suitable for the purposes of this experiment [Ref. 4].

At the start of each test, with the tunnel fan off, the wedge was wrapped with the heating pad, and brought up to temperatures of approximately 130°F. The pad was then removed, wind tunnel access doors closed, and the fan started. Runs were made at 50% and 75% fan speed, corresponding to 200 and 306 feet/second, respectively. Free stream velocities were calculated using the installed manometer, calibrated in inches H_2O. Free stream temperatures were determined by both a calibrated thermometer and a thermocouple inserted in the flow.

The cooling process was then recorded using the installed thermocouple output to the strip chart recorders, and the thermal imaging system connected to a video tape recorder for simultaneous data acquisition. In initial tests, the temperature sensitivity settings on the imaging system were selected at 5.0°F, which yielded an 80 degree range from 50°F to 130°F,

to view the entire cooling process. In subsequent tests, a sensitivity of 2.0°F was selected, giving a 32 degree range from 90°F to 122°F. This lower sensitivity/range setting was necessary to obtain a good agreement with the thermocouple data.

After a considerable amount of system testing, this process was undertaken four times at each of the two fan speeds for data evaluation and correlation.

B. DATA REDUCTION

Applying the formula for the lumped-capacitance analysis, the transient data from the thermocouple readings and the thermal imaging system were used to deduce the corresponding heat transfer coefficients. The calculations were performed using TK! SOLVER, a microcomputer spreadsheet [Ref. 5]. Tables 1 and 2 exhibit the program equations and variables, which provide not only the heat transfer coefficient, but also an estimate of the uncertainty of that calculation, and the corresponding Biot number, for each of the two sensor types. The uncertainty analysis of the heat transfer coefficient calculation is included as Appendix A.

The reduction of the thermocouple data was fairly straightforward, as the output was temperature versus time. However, reducing the thermal imaging system data required running the video tape recording frame by frame (each frame corresponding to 1/60 second) to determine the temperature at a given time.

This method generated the largest uncertainty in the calculation because the visual color bands and digital readout of the system changed only when the temperature of the body changed more than the sensitivity setting. For example, at a 5.0°F setting, the readout would persist for perhaps three seconds of test time before changing from 110°F to 105°F, while in reality, as displayed by the thermocouple readings, the surface temperature could be any temperature within this range at a particular instant. (This problem is analogous to that due to a large interval size in a finite-difference calculation.) There also existed occasions when, particularly at temperatures near thermal equilibrium, the readout would take relatively long periods of time to stabilize, which made determining the exact temperature/time data difficult. However, these difficulties were overcome by operator experience and use of the narrower sensitivity setting for correlating data in smaller segments rather than over the entire cooling span.

V. EXPERIMENTAL RESULTS

A. FLAT PLATE CORRELATION

The analysis of a flat plate of identical material, length, and width in identical flow conditions was used to attain a degree of confidence in the accuracy of the results of the wedge experiment. This analysis is based upon determining the Reynolds and Prandtl numbers for the flow, and solving the following equation for the average Nusselt number: [Ref. 6]

$$\overline{Nu} = 0.664\, Re^{1/2} Pr^{1/3}$$

The Nusselt number was then used to determine the average heat transfer coefficient from:

$$\bar{h} = \frac{\overline{Nu}\, k}{\ell}$$

where

ℓ = length of flat plate, ft.

These procedures resulted in a heat transfer coefficient of 22 BTU/hr-ft^2-°F for free stream velocity of 200 ft/sec, and 28 BTU/hr-ft^2-°F at velocity of 306 ft/sec. The results of this calculation are shown in Appendix B.

B. THERMOCOUPLE RESULTS

Using the strip chart recorder traces, the heat transfer coefficient at the surface thermocouple location was determined from the lumped-capacitance solution of exponential temperature decrease with time. For the free stream velocity of 200 ft/sec, h varied from 27.5 to 33.2 BTU/hr-ft^2-°F, with an average uncertainty band of ±1.75 BTU/hr-ft^2-°F. At velocity of 306 ft/sec, h had values ranging from 41.03 to 42.7 BTU/hr-ft^2-°F, with average uncertainty of ±1.80 BTU/hr-ft^2-°F. These calculations are shown in Tables 4-11.

C. THERMAL IMAGING SYSTEM RESULTS

As shown in Tables 12-19, using the same analysis and temperature range, h values were determined to be 27.7 to 33.5 BTU/hr-ft^2-°F, with an uncertainty band of ±1.9 BTU/hr-ft^2-°F for the lower free stream velocity, while values of 39.9 to 41.8 were obtained at higher speed. Figures 3 and 4 show the comparison of wedge surface temperature versus time for the two sensors at each velocity, and Figures 5 and 6 show the calculated values from each sensor versus time, again at each speed.

It is important to note that this measurement corresponds to conditions at a particular point on the wedge, that is, the location of the corresponding thermocouple. Further testing, with the cursor positioned at other points, would allow the development of a complete heat transfer map of the wedge surface. However, viewing of the entire wedge surface showed that

the transient isotherm variation was essentially uniform over a large portion of the surface (with the exception of narrow bands in the three-dimensional boundary layer regions near the sidewalls). Figure 7 is a still photograph of the wedge taken from the video output, which clearly exhibits this condition. Thus it may be deduced that the values determined above, at the thermocouple location, are representative of conditions over a major portion of the wedge surface. The ability to make such observations is a significant virtue of the infrared thermography method.

D. TVC VANE ANALYSIS

An actual TVC vane was received from NWC China Lake, Ca for analyzing the effect of complex geometry on convective heat transfer using the thermal imaging system.

This vane, shown in Figure 8, was constructed of copper-impregnated tungsten (80% W, 20% Cu), with the following material properties:

$$\rho = 1076.544 \frac{lbm}{ft^3} \qquad k = 148 \frac{BTU}{hr\text{-}ft\text{-}^\circ F} \qquad c = 0.037 \frac{BTU}{lbm\text{-}^\circ F}$$

The vane volume was calculated to be 2.295×10^{-5} ft^3, with a corresponding surface area of 1.5551×10^{-1} ft^2. All values were then entered into a formula sheet as before, shown in Table 3.

The vane was mounted on two aluminum stanchions with the same baseplate used by China Lake in their experiments. The

thermal imaging system was set up to view the vane through the side port of the subsonic wind tunnel with the IRTRAN optic window installed. The identical heating procedure was used, however, for reasons unknown, the pad would only reach 105°F. This was deemed sufficient, as it still gave a 40 degree temperature differential. The wind tunnel was operated at 50% flow speed (200 ft/sec).

Three test runs were performed, with the cursor at the midspan for runs 1 and 3, and on the leading edge at the baseplate boundary for run 2. The cursor was moved for run 2 to investigate and analyze a more rapid temperature gradient noticed in that area in the previous run. Run 1 yielded an average h of 41.5 BTU/hr-ft^2-°F ±3.23, run 2 yielded an average of 54.8 ±4.41, and run 3 gave an average of 42.4 ±3.9. The largest Biot number was calculated as 0.0063, well within the lumped-capacitance analysis criteria.

Figure 9 is a color thermograph of the vane during cooldown. As compared to the thermogram of the double wedge (Figure 7), the temperature map is fairly uniform over the body, with the exception of faster cooling at the leading and trailing edges, and an interesting area near the top of the vane below the apex. While vane thickness would explain the shape of most of the isotherms, the upper region undoubtedly is affected by a unique flow field, which increases the heat transfer coefficient by approximately 8% (Table 22). Tables 20-22 show the results of these tests, and Figures 10 and 11 are graphs of temperature and h versus time, respectively.

VI. CONCLUSIONS AND RECOMMENDATIONS

A. CONCLUSIONS

The results obtained from the thermal imaging system are, within a small experimental uncertainty, in agreement with the results of the thermocouples for all conditions tested here. Both experimental method's results were also sufficiently close to the theoretical flat plate solution to allow confidence in their accuracy, primarily due to the small wedge angle used.

The primary disadvantage of the thermal imaging system is the increase in size of the uncertainty band as the temperature sensitivity is widened. For large sensitivities of 5 degrees or more, the results become comparatively less accurate, again similar to using large step sizes in finite element calculations. Future users of this system in experiments similar to this one will have to adjust the sensitivity settings with respect to the overall temperature range desired, most likely by trial and error, to get the degree of accuracy required.

Nevertheless, the results obtained in this experiment lead to the conclusion that the thermal imaging system, when properly employed, would be a very good alternative to thermocouples in applications similar to this one. It provides accurate local and global readings with no need for

complicated data acquisition/reduction equipment and extensive instrumentation. The system is transportable, very reliable, and easy to operate. Although the system requires special infrared optic material for viewing models in an enclosed environment, several vendors were found who are capable of providing the material in various shapes and sizes at a reasonable expense in time and money.

B. RECOMMENDATIONS

The findings of this research lead to a recommendation for using this system for surface temperature measurements in the next phase of this project, using the wedge model in a supersonic wind tunnel for the same heat transfer coefficient calculation. This model was designed for ease of installation in the supersonic tunnel, when it becomes available, and an optic window has been obtained that will allow infrared viewing of the model while withstanding the environment (temperature and pressure differentials) in supersonic flow. Particular problems that might be encountered in supersonic applications include:

1) Sufficient difference in model and free stream temperatures to cause adequate heat transfer--the model may have to be heated prior to testing by some internal means (installation of wires for Joulean heating) to increase the recovery factor.

2) The on-site supersonic tunnel has a significantly smaller run-time available due to its pressure vessel configuration, thus yielding short run durations (a few minutes) and long (hours vice minutes) pressurization durations between tests.

3) As other model shapes and materials are considered, the necessity for maintaining the Biot number less than 0.1 could become critical, or another method

of analysis would have to be chosen if the lumped-capacitance assumption is not valid.

It is also recommended that the next experimenter familiarize himself with the system thoroughly, and invest time in viewing the video tape outputs of the system to get experience in temperature determination. This experience will prove to be a great factor in enhancing the accuracy of the results.

APPENDIX A

UNCERTAINTY ANALYSIS CALCULATIONS

$$\Theta = \frac{T - T_\infty}{T_o - T_\infty} = \exp - \left(\frac{hAt}{\rho c V}\right)$$ Formula used in calculation

$$h = \frac{- \ell n \Theta (\rho c V)}{A t},$$ solving for h

$$\therefore \quad h = F(\Theta, t, A, V, \rho, c)$$

$$\Delta h = \left[\left(\frac{\partial h}{\partial \Theta} \Delta\Theta\right)^2 + \left(\frac{\partial h}{\partial t} \Delta t\right)^2 + \left(\frac{\partial h}{\partial A} \Delta A\right)^2 + \left(\frac{\partial h}{\partial V} \Delta V\right)^2 + \left(\frac{\partial h}{\partial \rho} \Delta\rho\right)^2 + \left(\frac{\partial h}{\partial c} \Delta c\right)^2\right]^{1/2}$$

where Δ's are the uncertainty of the measured quantities.

$$(1) \quad \frac{\partial h}{\partial \Theta} \Delta\Theta = - \frac{\rho c V}{\Theta A t}\left[\left(- \frac{N}{D^2} \Delta D\right)^2 + \left(\frac{1}{D} \Delta N\right)^2\right]^{1/2}$$

where:

$$N = T - T_\infty, \quad D = T_o - T_\infty, \quad \Delta N = \left(\Delta T^2 + \Delta T_\infty^2\right)^{1/2},$$

$$\Delta D = \left(\Delta T_o^2 + \Delta T_\infty^2\right)^{1/2}, \quad \Delta T_\infty = 1.0 \ ^\circ F, \quad \Delta T_o = 1.0 \ ^\circ F$$

ΔT = 2.0 °F for IR data, ΔT = 1.0 °F for thermocouple data

$$(2)\quad \frac{\partial h}{\partial t}\Delta t = -\frac{\ell n\ \Theta\ \rho c V}{A t^2}\Delta t,$$

where:

$$\Delta t = 0.1 \text{ seconds} = 2.7778 \text{ E } -5 \text{ hours}$$

from IR system timer precision.

$$(3)\quad \frac{\partial h}{\partial A}\Delta A = -\frac{\ell n\ \Theta\ \rho c\ V}{A^2 t}\Delta A$$

where:

$$\Delta A = 0.001 \text{ in}^2 = 6.9444\text{E-}6\text{ft}^2$$

from machining precision.

$$(4)\quad \frac{\partial h}{\partial V}\Delta V = -\frac{\ell n\ \Theta\ \rho c}{A\ t}\Delta V,$$

where:

$$\Delta V = 1.0\text{E-}9 \text{ in}^3 = 5.7878\text{E-}13 \text{ ft}^3$$

from machining precision.

$$(5)\quad \frac{\partial h}{\partial \rho}\Delta \rho = -\frac{\ell n\ \Theta c\ V}{A t}\Delta \rho,$$

where:

$$\Delta \rho = 6.9082 \frac{\text{lbm}}{\text{ft}^3} \text{ [Ref. 7]}$$

$$(6) \quad \frac{\partial h}{\partial c} \Delta c = - \frac{\ell n\ \Theta\ \rho V}{A\ t} \Delta c,$$

where:

$$\Delta c = 0.001 \frac{BTU}{lbm\text{-}^{\circ}F} \text{ [Ref. 7]}$$

All above equations were included in the data reduction programs to solve for the uncertainty in h (delh).

APPENDIX B

FLAT PLATE SOLUTION

Given: $T_\infty = 60°F = 520°R \qquad 1"H_2O = 0.0361 \text{ psi}$

Find: $\bar{h}$ from the empirical flat plate in parallel flow equation:

$$\overline{Nu} = 0.664\, Re_x^{1/2}\, Pr^{1/3}$$

[Ref. 6]

$$\bar{h} = \frac{\overline{Nu}\, k}{L}$$

(1) Re_x: For $T_\infty = 520°R$: [Ref. 7]

$$\mu_{air} = 1.2039E\text{-}5 \frac{lbm}{ft\text{-}sec} \qquad Pr = 0.71 \qquad k = 0.01561 \frac{BTU}{hr\text{-}ft\text{-}°F}$$

$$\gamma_{air} = 0.0743 \frac{lbm}{ft^3} \qquad x = 2.50 \text{ in} = 0.2083 \text{ ft}$$

$$U_\infty^2 = \frac{\Delta p\, 2g}{\gamma} = \frac{(8.9"H_2O)(0.0361)(64.348)(144)}{0.0743}$$

$$U_\infty^2 = 40080.4 \frac{ft^2}{s^2}, \qquad U_\infty = 200.2 \frac{ft}{s}$$ for experimental low speed flow

For $\Delta p = 20.8"\ H_2O$, $U_\infty = 306.1 \frac{ft}{s}$ for experimental high speed flow

$$Re_x = \frac{\gamma U_\infty x}{\mu} = \frac{(0.0743)(200.2)(0.2083)}{1.2039E\text{-}5} = 2.573E5$$

$$Re_x = \frac{(0.0743)(306.1)(0.2083)}{1.2039E\text{-}5} = 3.935E5$$

Assuming Re_{crit} = 5.0E5, laminar flow conditions exist in both cases.

(2) $\overline{Nu}$: For low speed flow:

$$\overline{Nu} = 0.664(2.574E5)^{1/2}(0.71)^{1/3}) = 300.5$$

For high speed flow:

$$\overline{Nu} = 0.664(3.935E5)^{1/2}(0.71)^{1/3} = 371.6$$

(3) $\bar{h}$: For low speed flow:

$$\bar{h} = \frac{\overline{Nu}\, k}{x} = \frac{(300.5)(0.01561)}{0.2083} = 22.5 \frac{BTU}{hr\text{-}ft^2\text{-}°F}$$

For high speed flow:

$$\bar{h} = \frac{\overline{Nu}\, k}{x} = \frac{(371.6)(0.01561)}{0.2083} = 27.8 \frac{BTU}{hr\text{-}ft^2\text{-}°F}$$

APPENDIX C

TABLES

TABLE 1

FORMULA SHEET FOR THERMOCOUPLE DATA REDUCTION

St	Input	Name	Output	Unit	Comment
L		theta			dimensionless temperature
L		Tt		F	temperature at time t
		Tinf		F	free stream temperature
		Ti		F	initial wedge temperature
L		h		$\frac{btu}{hr\text{-}ft^2\text{-}°F}$	heat transfer coefficient
L		delh		$\frac{btu}{hr\text{-}ft^2\text{-}°F}$	uncertainty in h value
	.27777778	a		ft^2	wedge wetted perimeter
L		t		hours	
	558	ro		lbm/ft^3	copper density
	.091	c		btu/lb-F	specific heat capacity
	.00346013	V		ft^3	wedge volume
L		q		btu/hr	heat transfer
	230	k		$\frac{btu}{hr\text{-}ft\text{-}°F}$	wedge conductivity
L		BIOT			
L		time		seconds	
		u			(dh/dtheta)*(delta theta)
		vv			(dh/dt)*(delta t)
		w			(dh/dA)*(delta a)
		x			(dh/dV)*(delta V)
		y			(dh/dro)*(delta ro)
		z			(dh/dc)*(delta c)

TABLE 1 (CONTINUED)

S Rule

* theta = $\frac{(Tt-Tinf)}{(Ti-Tinf)}$

* theta = exp $\frac{(-(h*a*t)}{(ro*c*V))}$

* q = h*a*(Tt-Tinf)

* BIOT = $\frac{h*V}{(k*a)}$

* time = t*3600

* u = (ro*c*V)/(theta*at))*((1.4142*(Tt-Tinf)/(Ti-Tinf)^2)
+ (1.8868/(Ti-Tinf))^2)

* vv = (2.777777e-5*ln(theta)*ro*c*V/(a*t^2))

* w = (ln(theta)*ro*c*V*6.9444e-6/(a^2*t))

* x = (ln(theta)*ro*c*5.787e-13/(a*t))

* y = (ln(theta)*c*V*6.9082/(a*t))

* z = (ln(theta)*V*ro*.001/(a*t))

* delh = sqrt (u^2+vv^2+w^2+x^2+y^2+z^2)

TABLE 2

FORMULA SHEET FOR INFRARED SYSTEM DATA REDUCTION

St	Input	Name	Output	Unit	Comment
L		theta			dimensionless temperature
L		Tt		F	temperature at time t
		Tinf		F	free stream temperature
		Ti		F	initial wedge temperature
L		h		$\frac{btu}{hr\text{-}ft^2\text{-}°F}$	heat transfer coefficient
L		delh		$\frac{btu}{hr\text{-}ft^2\text{-}°F}$	uncertainty in h value
	.27777778	a		ft^2	wedge wetted perimeter
L		t		hours	
	558	ro		lbm/ft^3	copper density
	.091	c		btu/lb-F	specific heat capacity
	.00346013	V		ft^3	wedge volume
L		q		btu/hr	heat transfer
	230	k		$\frac{btu}{hr\text{-}ft\text{-}°F}$	wedge conductivity
L		BIOT			
L		time		seconds	
		u			(dh/dtheta)*(delta theta)
		vv			(dh/dt)*(delta t)
		w			(dh/dA)*(delta a)
		x			(dh/dV)*(delta V)
		y			(dh/dro)*(delta ro)
		z			(dh/dc)*(delta c)

S Rule

* $\text{theta} = \frac{(Tt-Tinf)}{(Ti-Tinf)}$

* $\text{theta} = \exp\left(\frac{-(h*a*t)}{(ro*c*V)}\right)$

* q = h*a*(Tt-Tinf)

TABLE 2 (CONTINUED)

* BIOT = $\frac{h*V}{(k*a)}$

* time = t*3600

* u = (ro*c*V/(theta*a*t))*((1.4142*(Tt-Tinf)/(Ti-Tinf)^2)
+ (2.2361/(Ti-Tinf))^2)

* vv = (2.777777e-5*ln(theta)*ro*c*V/(a*t^2))

* w = (ln(theta)*ro*c*V*6.9444e-6/(a^2*t))

* x = (ln(theta)*ro*c*5.787e-13/(a*t))

* y = (ln(theta)*c*V*6.9082/(a*t))

* z = (ln(theta)*V*ro*.001/(a*t))

* delh = sqrt(u^2+vv^2+w^2+x^2+y^2+z^2)

TABLE 3

FORMULA SHEET FOR TVC VANE DATA REDUCTION

S Rule

* theta = $\frac{(Tt-Tinf)}{(Ti-Tinf)}$

* theta = exp($\frac{-(h*a*t)}{(ro*c*V)}$)

* q = h*a*(Tt-Tinf)

* BIOT = $\frac{h*V}{(k*a)}$

* time = t*3600

* u = (ro*c*V/(theta*a*t))*((1.4142*(Tt-Tinf)/(Ti-Tinf)^2)
+ (2.2361/(Ti-Tinf))^2)

* vv = (2.777777e-5*ln(theta)*ro*c*V/(a*t^2))

* w = (ln(theta)*ro*c*V*6.9444e-6/(a^2*t))

* x = (ln(theta)*ro*c*5.787e-13/(a*t))

* y = (ln(theta)*c*V*6.9082/(a*t))

* z = (ln(theta)*V*ro*.001/(a*t))

* delh = sqrt(u^2+vv^2+w^2+x^2+y^2+z^2)

TABLE 3 (CONTINUED)

St	Input	Name	Output	Unit	Comment
L		theta			dimensionless temperature
L	81	Tt		F	temperature at time t
	61	Tinf		F	free stream temperature
	97	Ti		F	initial TVC vane temperature
L		h		$\frac{btu}{hr\text{-}ft^2\text{-}°F}$	heat transfer coefficient
L		delh			uncertainty in h value
	.155507	a		ft^2	TVC vane surface area
L		t		hours	
	1076.544	ro		lbm/ft^3	TVC vane density-80% W, 20% Cu
	.037	c		btu/lb-F	specific heat capacity
	.00229545	V		ft^3	TVC vane volume
L		q		btu/hr	heat transferred
	148	k		$\frac{btu}{hr\text{-}ft\text{-}°F}$	TVC vane conductivity
L		BIOT			
L	47.3	time		seconds	

TABLE 4

RESULTS OF THERMOCOUPLE CALCULATIONS, LOW TUNNEL SPEED

Run: #1

Tunnel Air Velocity: 201.3 $\frac{ft}{sec}$

Average Biot Number: 0.00164

Average Uncertainty in h: $\pm$ 2.28 $\frac{btu}{hr\text{-}ft^2\text{-}°F}$

Time (Seconds)	Temperature (°F)	h ($\frac{btu}{hr\text{-}ft\text{-}°F}$)
0.0	117.5	____
6.7	112.5	30.92
14.5	107.5	30.00
22.7	102.5	30.32
32.0	97.5	30.42
43.0	92.5	30.21
55.0	87.5	30.54

TABLE 5

RESULTS OF THERMOCOUPLE CALCULATIONS, LOW TUNNEL SPEED

Run: #2

Tunnel Air Velocity: 193.3 $\frac{ft}{sec}$

Average Biot Number: 0.00156

Average Uncertainty in h: $\pm$ 1.95 $\frac{btu}{hr\text{-}ft^2\text{-}°F}$

Time (Seconds)	Temperature (°F)	h ($\frac{btu}{hr\text{-}ft\text{-}°F}$)
0.0	114.5	____
3.5	112.5	24.32
5.6	110.5	30.99
9.3	108.5	28.56
12.8	106.5	28.24
16.0	104.5	28.85
21.0	102.5	26.97
24.6	100.5	27.48

TABLE 6

RESULTS OF THERMOCOUPLE CALCULATION, LOW TUNNEL SPEED

Run: #3

Tunnel Air Velocity: 197.6 $\frac{ft}{sec}$

Average Biot Number: 0.00159

Average Uncertainty in h: $\pm$ 1.53 $\frac{btu}{hr\text{-}ft^2\text{-}°F}$

Time (Seconds)	Temperature (°F)	h ($\frac{btu}{hr\text{-}ft\text{-}°F}$)
0.0	120.0	____
10.0	113.3	28.70
20.0	107.0	29.47
30.0	101.7	29.39
40.0	96.7	29.92
50.0	92.8	29.54
60.0	89.2	29.54

TABLE 7

RESULTS OF THERMOCOUPLE CALCULATIONS, LOW TUNNEL SPEED

Run: #4

Tunnel Air Velocity: 207.9 $\frac{ft}{sec}$

Average Biot Number: 0.00182

Average Uncertainty in h: $\pm$ 2.41 $\frac{btu}{hr\text{-}ft^2\text{-}°F}$

Time (Seconds)	Temperature (°F)	h ($\frac{btu}{hr\text{-}ft\text{-}°F}$)
0.0	111.0	____
5.0	107.7	32.44
10.0	104.3	34.23
15.0	101.4	33.72
20.0	98.7	33.71
25.0	96.2	33.69
30.0	93.7	33.82
35.0	91.6	33.57
37.0	91.0	33.17

TABLE 8

RESULTS OF THERMOCOUPLE CALCULATIONS, HIGH TUNNEL SPEED

Run: #5

Tunnel Air Velocity: 308.2 $\frac{ft}{sec}$

Average Biot Number: 0.0022

Average Uncertainty in h: $\pm$ 1.88 $\frac{btu}{hr\text{-}ft^2\text{-}°F}$

Time (Seconds)	Temperature (°F)	h ($\frac{btu}{hr\text{-}ft\text{-}°F}$)
0.0	119.0	____
5.0	114.3	40.37
10.0	109.7	41.45
15.0	105.5	41.73
20.0	101.7	41.95
25.0	98.3	42.03
30.0	95.2	42.00
35.0	92.2	42.26
37.0	91.0	42.66

TABLE 9

RESULTS OF THERMOCOUPLE CALCULATIONS, HIGH TUNNEL SPEED

Run: #6

Tunnel Air Velocity: 303.8 $\frac{ft}{sec}$

Average Biot Number: 0.0022

Average Uncertainty in h: $\pm$ 2.11 $\frac{btu}{hr\text{-}ft^2\text{-}°F}$

Time (Seconds)	Temperature (°F)	h ($\frac{btu}{hr\text{-}ft\text{-}°F}$)
0.0	119.0	____
5.0	114.5	38.15
10.0	110.3	38.64
15.0	106.7	37.48
20.0	102.1	40.84
25.0	98.5	41.52
30.0	95.6	41.07
35.0	92.4	41.88
38.0	91.0	41.54

TABLE 10

RESULTS OF THERMOCOUPLE CALCULATIONS, HIGH TUNNEL SPEED

Run: #7

Tunnel Air Velocity: 306.0 $\frac{ft}{sec}$

Average Biot Number: 0.0022

Average Uncertainty in h: $\pm$ 2.28 $\frac{btu}{hr\text{-}ft^2\text{-}°F}$

Time (Seconds)	Temperature (°F)	h ($\frac{btu}{hr\text{-}ft\text{-}°F}$)
0.0	119.0	____
5.0	114.4	38.06
10.0	110.0	39.13
15.0	105.7	40.30
20.0	102.0	40.32
25.0	98.5	40.70
30.0	95.4	40.57
35.0	91.4	43.12
37.5	91.0	41.03

TABLE 11

RESULTS OF THERMOCOUPLE CALCULATIONS, HIGH TUNNEL SPEED

Run: #8

Tunnel Air Velocity: 306.0 $\frac{ft}{sec}$

Average Biot Number: 0.0022

Average Uncertainty in h: $\pm$ 1.96 $\frac{btu}{hr\text{-}ft^2\text{-}°F}$

Time (Seconds)	Temperature (°F)	h ($\frac{btu}{hr\text{-}ft\text{-}°F}$)
0.0	119.0	____
5.0	114.4	39.57
10.0	110.0	39.89
15.0	105.8	40.81
20.0	102.2	40.61
25.0	98.6	41.18
30.0	95.5	41.23
35.0	92.5	41.70
38.0	91.0	41.53

TABLE 12

RESULTS OF INFRARED SYSTEM CALCULATIONS, LOW TUNNEL SPEED

Run: #1

Tunnel Air Velocity: 201.3 $\frac{ft}{sec}$

Average Biot Number: 0.00164

Average Uncertainty in h: $\pm$ 1.88 $\frac{btu}{hr\text{-}ft^2\text{-}°F}$

Time (Seconds)	Temperature (°F)	h ($\frac{btu}{hr\text{-}ft\text{-}°F}$)
0.0	117.5	____
6.1	112.5	33.96
13.0	107.5	33.46
22.0	102.5	31.29
31.5	97.5	30.90
41.7	92.5	31.15
52.5	87.5	31.99

TABLE 13

RESULTS OF INFRARED SYSTEM CALCULATIONS, LOW TUNNEL SPEED

Run: #2

Tunnel Air Velocity: 193.3 $\frac{ft}{sec}$

Average Biot Number: 0.00151

Average Uncertainty in h: $\pm$ 2.16 $\frac{btu}{hr\text{-}ft^2\text{-}°F}$

Time (Seconds)	Temperature (°F)	h ($\frac{btu}{hr\text{-}ft\text{-}°F}$)
0.0	114.5	____
3.1	112.5	28.40
6.1	110.5	28.46
9.5	108.5	27.96
13.3	106.5	27.18
17.0	104.5	27.15
21.5	102.5	27.33
24.4	100.5	27.71

TABLE 14

RESULTS OF INFRARED SYSTEM CALCULATIONS, LOW TUNNEL SPEED

Run: #3

Tunnel Air Velocity: 197.6 $\frac{ft}{sec}$

Average Biot Number: 0.00161

Average Uncertainty in h: $\pm$ 1.98 $\frac{btu}{hr\text{-}ft^2\text{-}°F}$

Time (Seconds)	Temperature (°F)	h ($\frac{btu}{hr\text{-}ft\text{-}°F}$)
0.0	119.0	____
5.5	115.0	30.68
11.5	111.0	30.52
18.9	107.0	29.05
26.5	103.0	28.91
32.3	99.0	31.15
40.4	95.0	31.54
50.4	91.0	31.32

TABLE 15

RESULTS OF INFRARED SYSTEM CALCULATIONS, LOW TUNNEL SPEED

Run: #4

Tunnel Air Velocity: 207.9 $\frac{ft}{sec}$

Average Biot Number: 0.0018

Average Uncertainty in h: $\pm$ 2.14 $\frac{btu}{hr\text{-}ft^2\text{-}°F}$

Time (Seconds)	Temperature (°F)	h ($\frac{btu}{hr\text{-}ft\text{-}°F}$)
0.0	111.0	____
2.8	109.0	34.61
6.0	107.0	33.02
9.4	105.0	32.35
12.4	103.0	33.48
16.3	101.0	32.64
19.3	99.0	33.94
22.8	97.0	34.44
27.0	95.0	34.19
31.8	93.0	33.65
36.6	91.0	33.53

TABLE 16

RESULTS OF INFRARED SYSTEM CALCULATIONS, HIGH TUNNEL SPEED

Run: #5

Tunnel Air Velocity: 308.2 $\frac{ft}{sec}$

Average Biot Number: 0.0021

Average Uncertainty in h: $\pm$ 1.85 $\frac{btu}{hr\text{-}ft^2\text{-}°F}$

Time (Seconds)	Temperature (°F)	h ($\frac{btu}{hr\text{-}ft\text{-}°F}$)
0.0	119.0	____
4.7	115.0	35.91
8.9	111.0	39.44
13.7	107.0	40.08
19.3	103.0	39.70
23.8	99.0	42.27
29.6	95.0	43.05
37.8	91.0	41.75

TABLE 17

RESULTS OF INFRARED SYSTEM CALCULATIONS, HIGH TUNNEL SPEED

Run: #6

Tunnel Air Velocity: 303.8 $\frac{ft}{sec}$

Average Biot Number: 0.0018

Average Uncertainty in h: $\pm$ 1.77 $\frac{btu}{hr\text{-}ft^2\text{-}°F}$

Time (Seconds)	Temperature (°F)	h ($\frac{btu}{hr\text{-}ft\text{-}°F}$)
0.0	119.0	____
5.9	115.0	35.45
10.8	111.0	37.69
16.2	107.0	36.91
21.6	103.0	35.47
26.5	99.0	37.97
32.7	95.0	38.97
39.6	91.0	39.86

TABLE 18

RESULTS OF INFRARED SYSTEM CALCULATIONS, HIGH TUNNEL SPEED

Run: #7

Tunnel Air Velocity: 306.0 $\frac{ft}{sec}$

Average Biot Number: 0.0021

Average Uncertainty in h: $\pm$ 1.86 $\frac{btu}{hr\text{-}ft^2\text{-}°F}$

Time (Seconds)	Temperature (°F)	h ($\frac{btu}{hr\text{-}ft\text{-}°F}$)
0.0	119.0	____
5.0	115.0	36.14
9.0	111.0	38.26
14.0	107.0	38.45
18.9	103.0	39.70
24.0	99.0	41.00
29.7	95.0	41.90
36.8	91.0	41.81

TABLE 19

RESULTS OF INFRARED SYSTEM CALCULATIONS, HIGH TUNNEL SPEED

Run: #8

Tunnel Air Velocity: 306.0 $\frac{ft}{sec}$

Average Biot Number: 0.0022

Average Uncertainty in h: $\pm$ 1.83 $\frac{btu}{hr\text{-}ft^2\text{-}°F}$

Time (Seconds)	Temperature (°F)	h ($\frac{btu}{hr\text{-}ft\text{-}°F}$)
0.0	119.0	____
4.9	115.0	37.14
10.3	111.0	37.46
14.7	107.0	37.45
20.6	103.0	37.20
25.9	99.0	38.85
31.5	95.0	40.45
38.2	91.0	41.32

TABLE 20

RESULTS OF TVC VANE CALCULATIONS

Run: #1

Tunnel Air Velocity: 214.3 $\frac{ft}{sec}$

Average Biot Number: 0.0041

Average Uncertainty in h: $\pm$ 3.23 $\frac{btu}{hr\text{-}ft^2\text{-}°F}$

Time (Seconds)	Temperature (°F)	h ($\frac{btu}{hr\text{-}ft\text{-}°F}$)
0.0	99.0	———
5.5	95.0	38.52
10.8	91.0	41.41
17.0	87.0	41.89
23.5	83.0	43.19
31.6	79.0	43.31
42.2	75.0	42.50

TABLE 21

RESULTS OF TVC VANE CALCULATIONS

Run: #2

Tunnel Air Velocity: 220.5 $\frac{ft}{sec}$

Average Biot Number: 0.0053

Average Uncertainty in h: $\pm$ 4.41 $\frac{btu}{hr\text{-}ft^2\text{-}°F}$

Time (Seconds)	Temperature (°F)	h ($\frac{btu}{hr\text{-}ft\text{-}°F}$)
0.0	97.0	———
4.0	93.0	62.33
9.0	89.0	59.10
16.4	85.0	52.33
23.2	81.0	53.63
33.0	77.0	52.01
47.3	73.0	49.17

TABLE 22

RESULTS OF TVC VANE CALCULATIONS

Run: #3

Tunnel Air Velocity: 220.5 $\frac{ft}{sec}$

Average Biot Number: 0.0042

Average Uncertainty in h: $\pm$ 3.90 $\frac{btu}{hr\text{-}ft^2\text{-}°F}$

Time (Seconds)	Temperature (°F)	h ($\frac{btu}{hr\text{-}ft\text{-}°F}$)
0.0	97.0	____
6.2	93.0	41.43
13.0	89.0	42.25
21.7	85.0	40.95
28.7	81.0	45.06
40.4	77.0	44.39

APPENDIX D

FIGURES

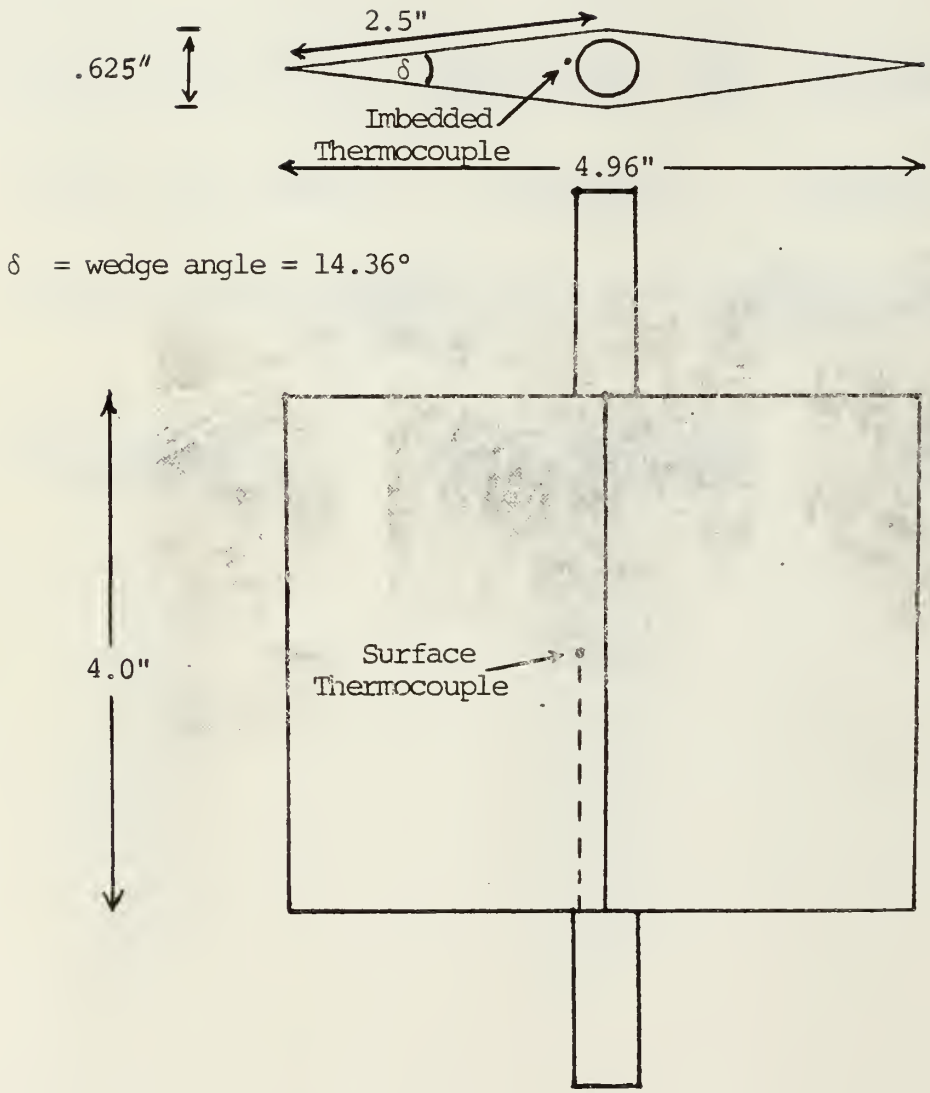

Figure 1. Diagram of Wedge Model

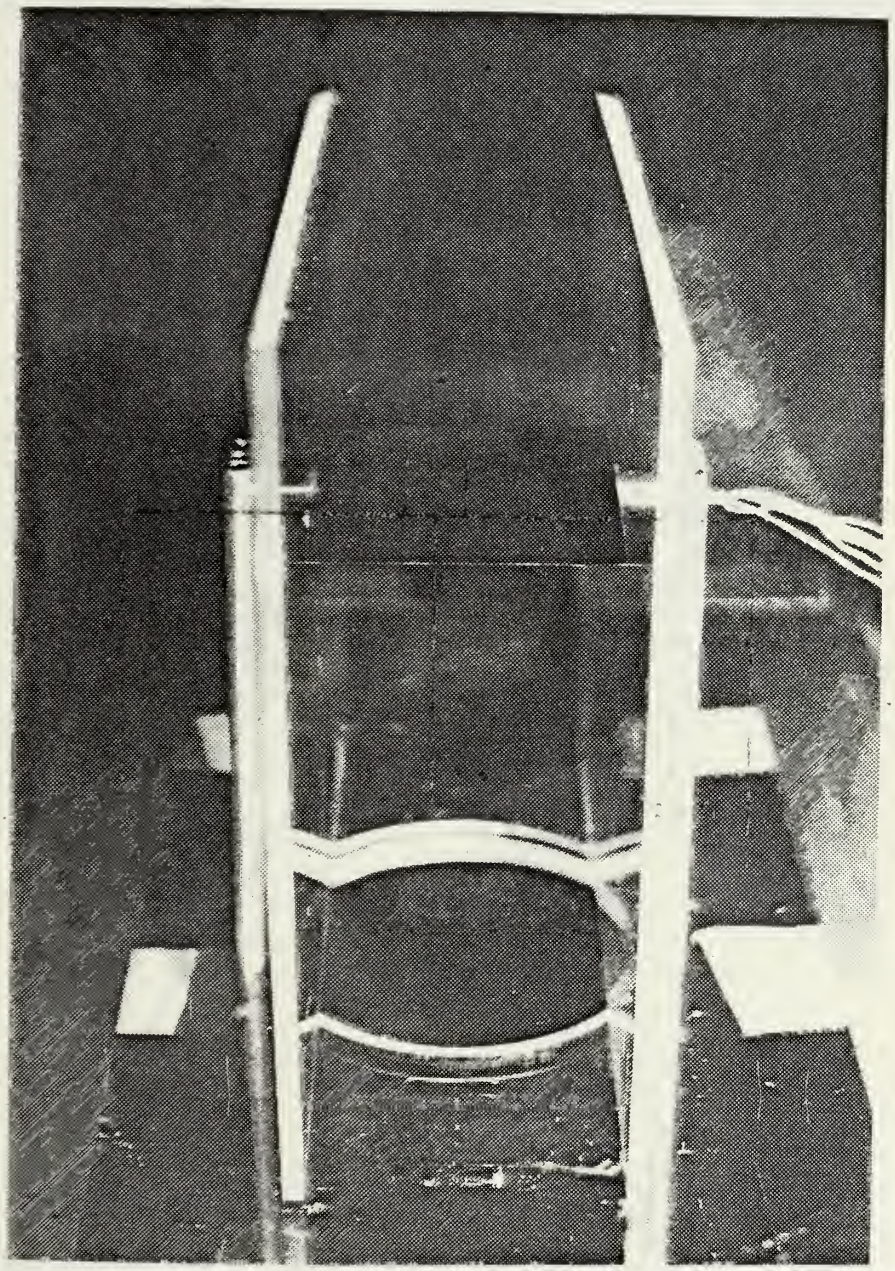

Figure 2. Rear View of Wedge Model Assembly

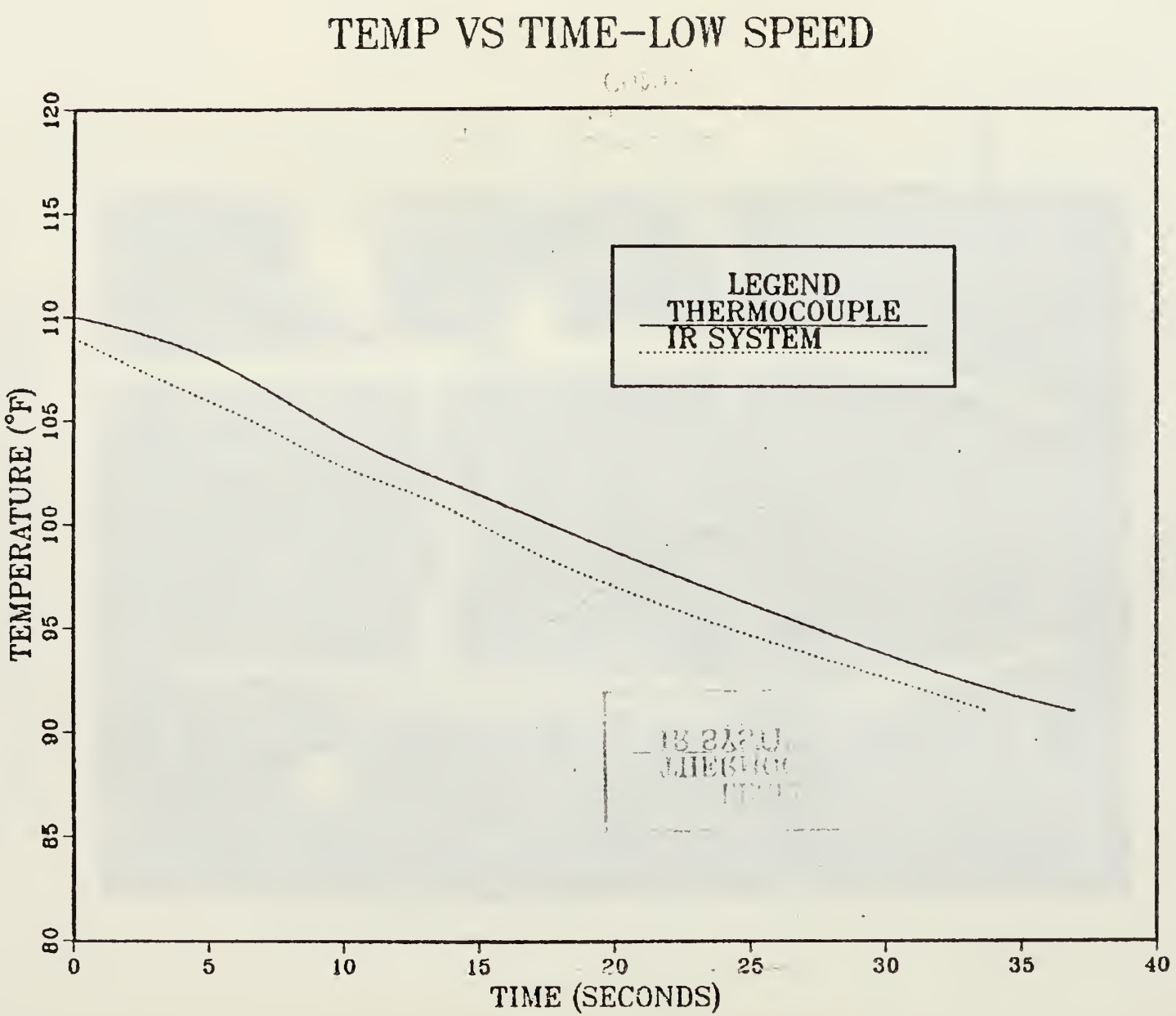

Figure 3. Graph of Wedge Temperature vs Time, Low Speed Flow

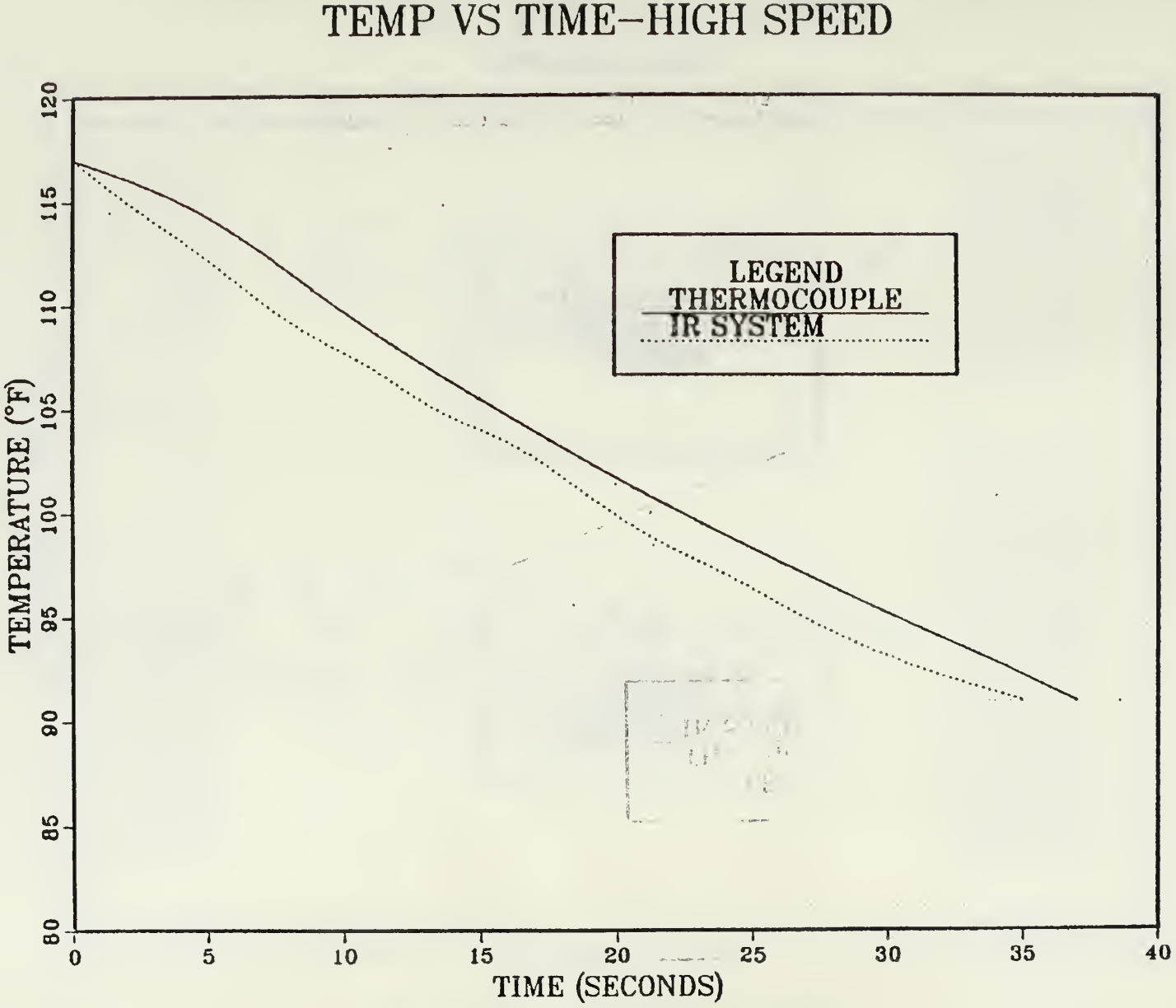

Figure 4. Graph of Wedge Temperature vs Time, High Speed Flow

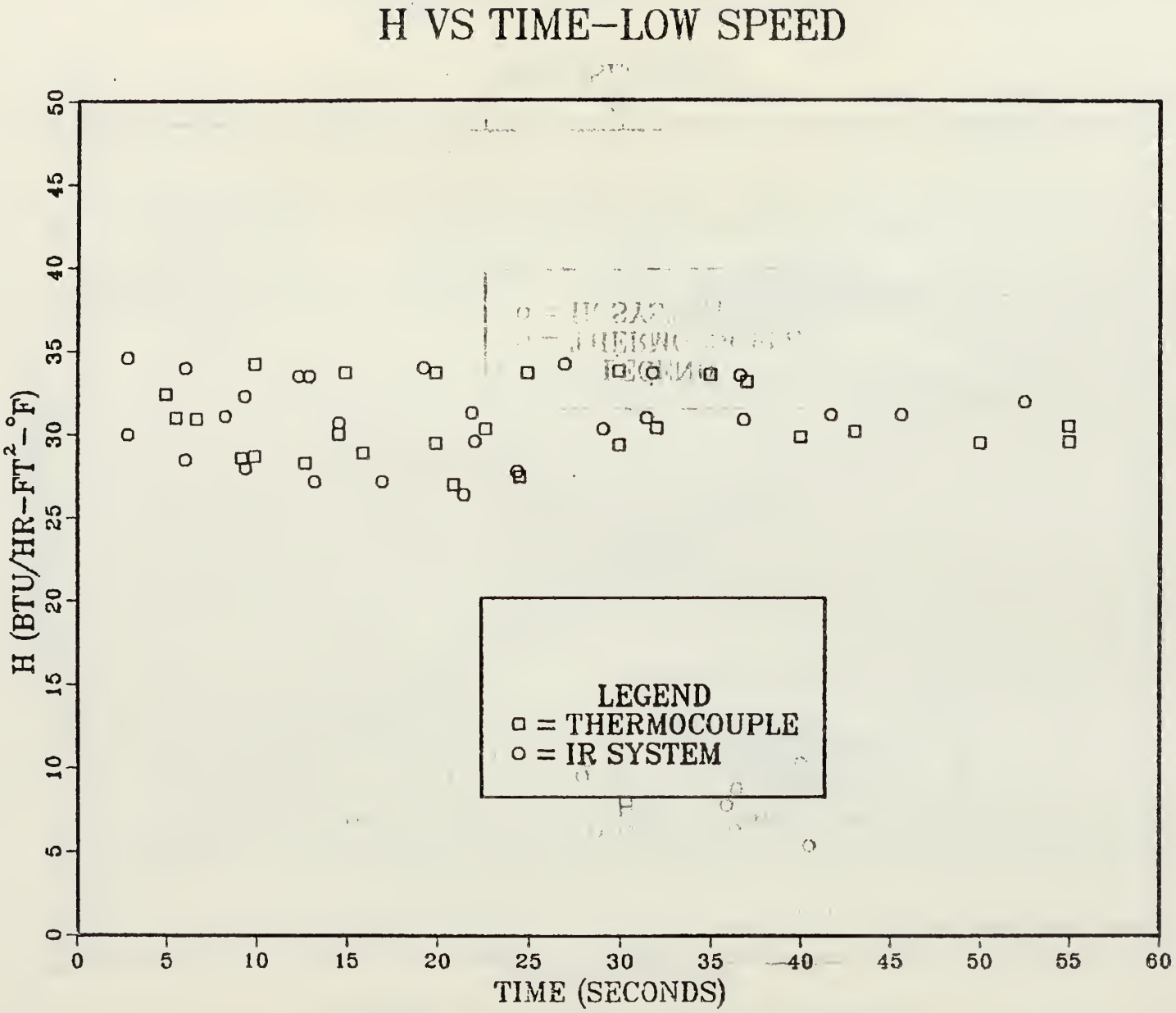

Figure 5. Graph of Wedge h vs Time, Low Speed Flow

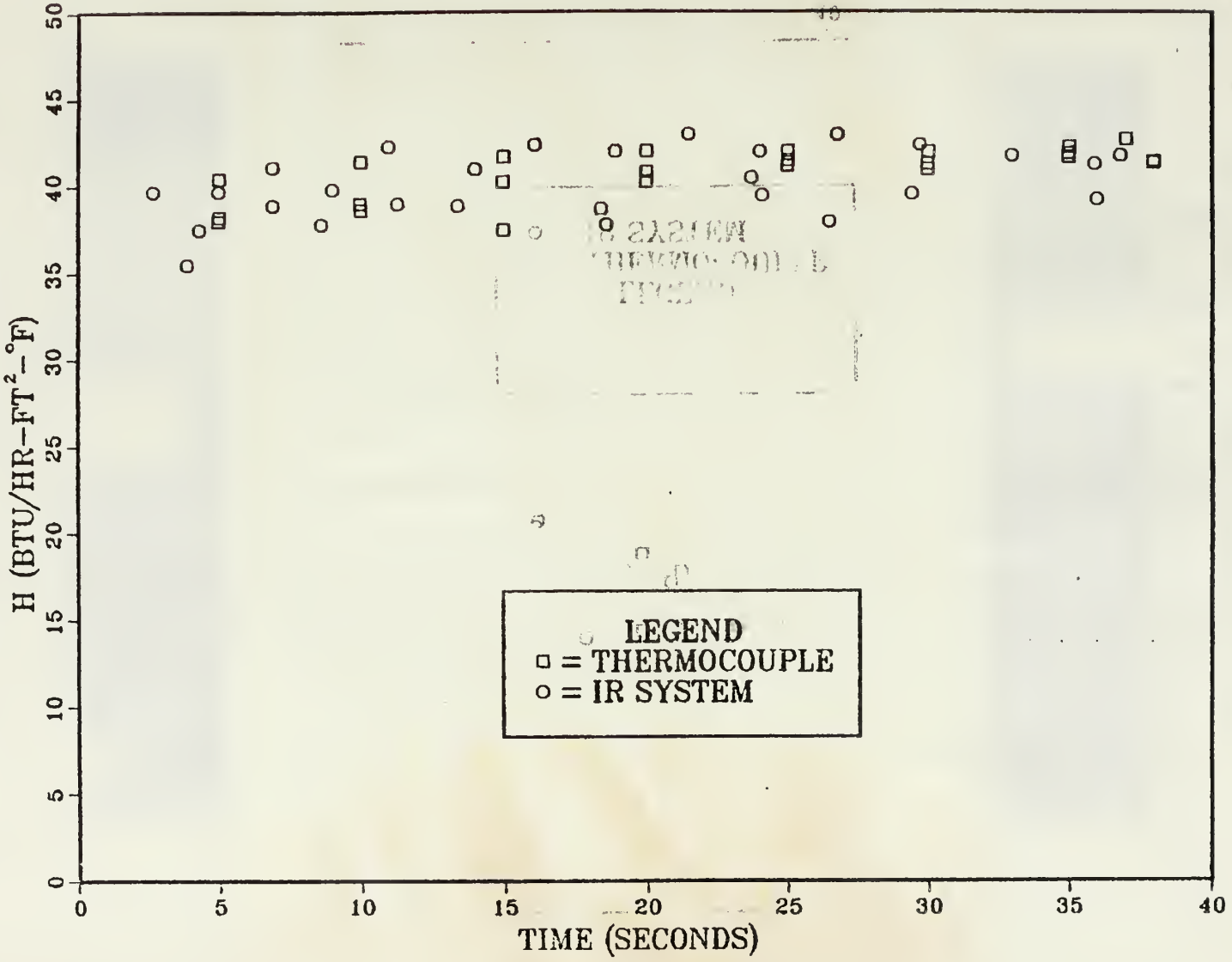

Figure 6. Graph of Wedge h vs Time, High Speed Flow

Flow Direction Relative to Picture

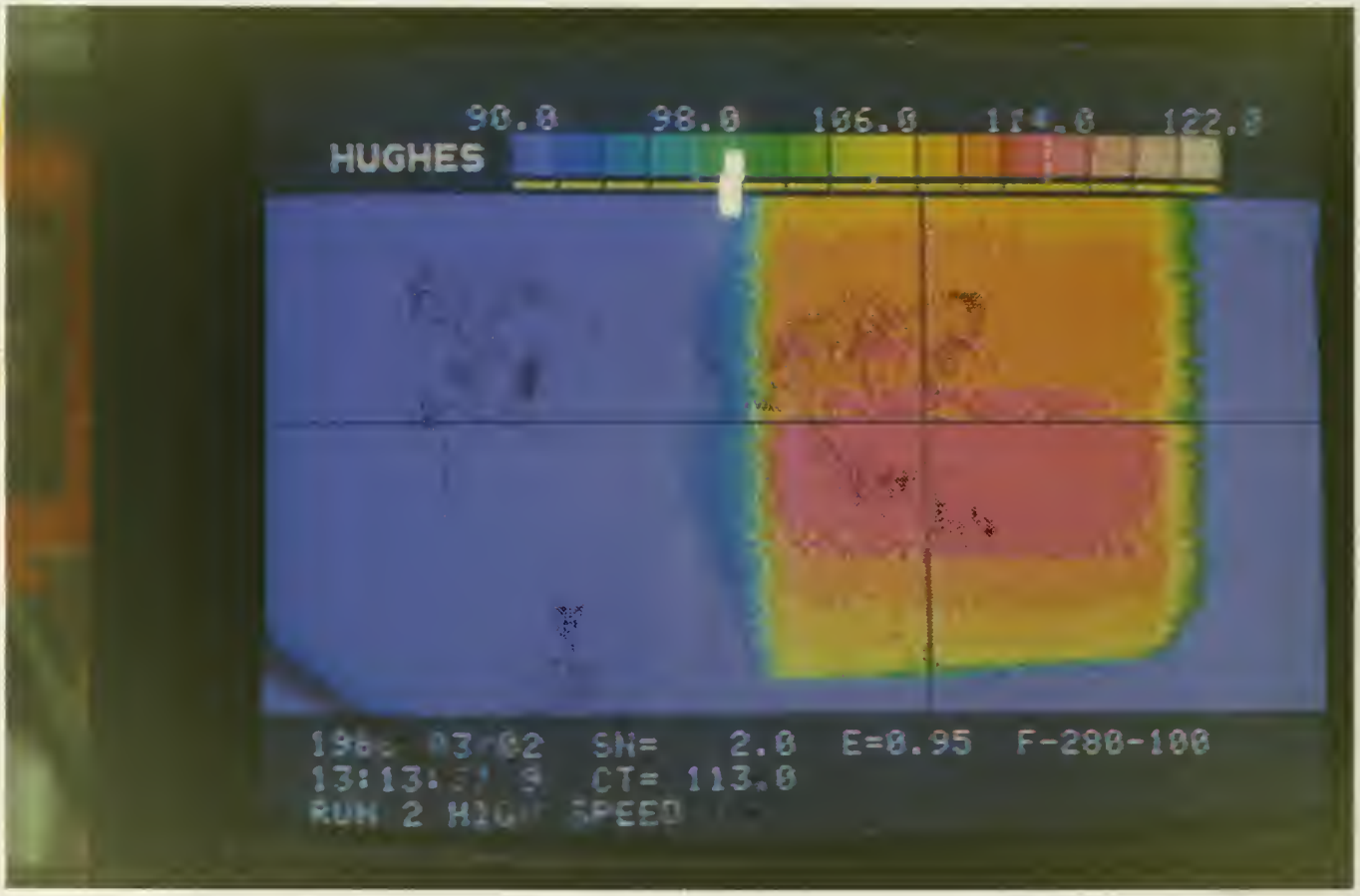

Figure 7. Color Thermogram of Wedge

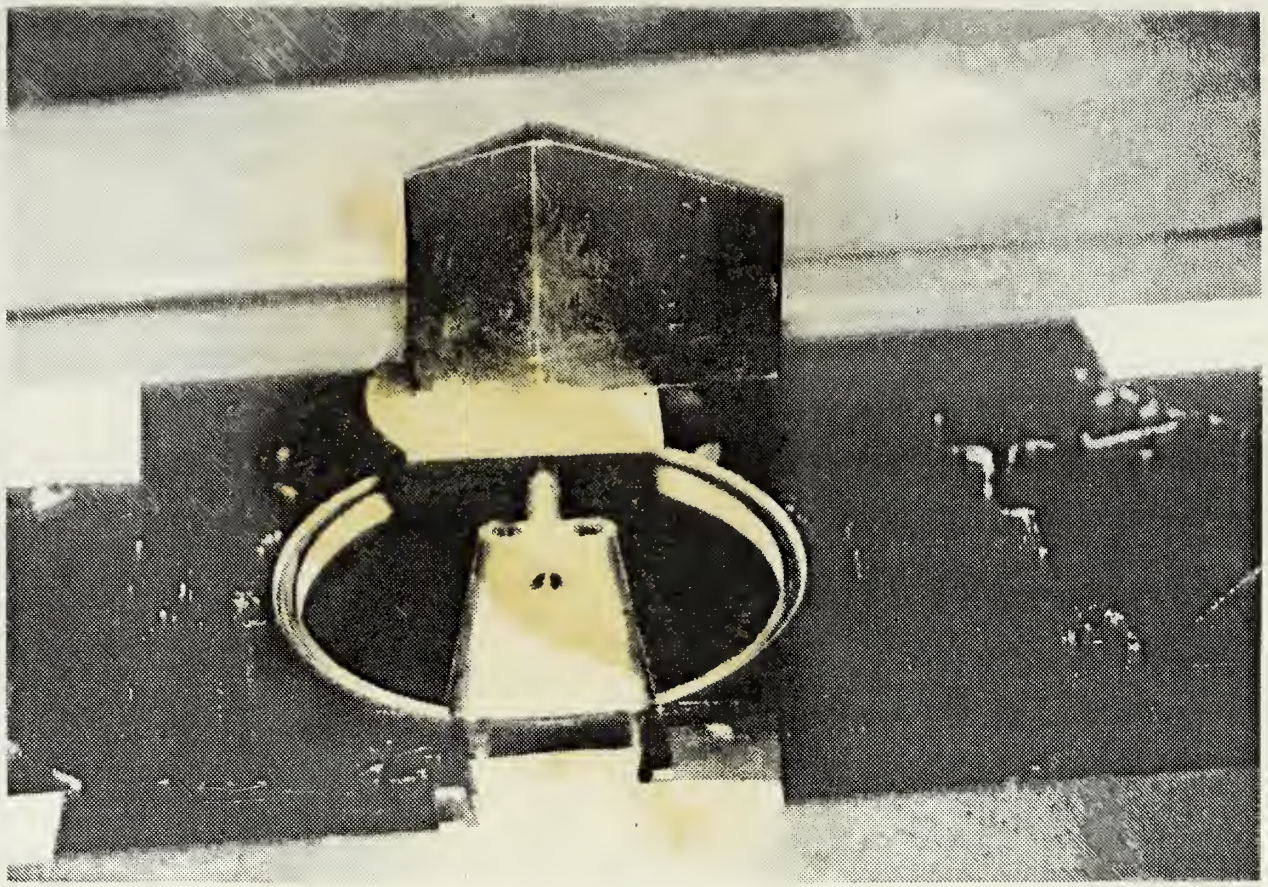

Figure 8. Photograph of TVC Vane

Flow Direction

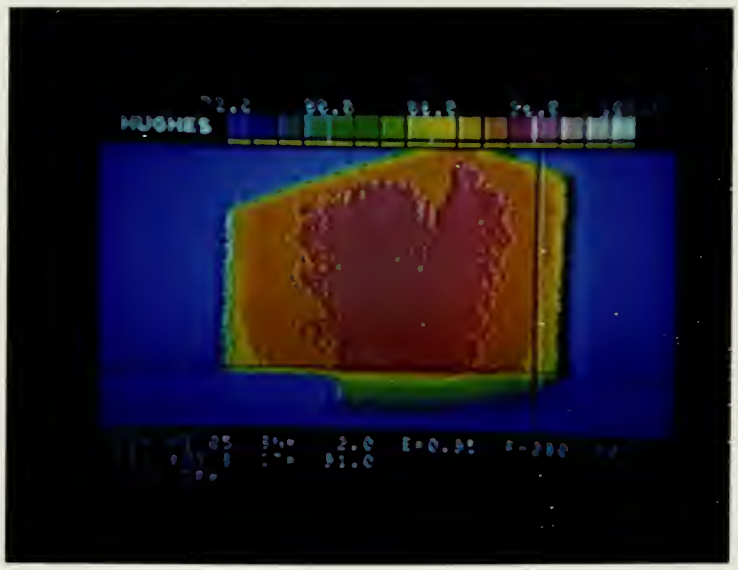

Figure 9. Color Thermogram of TVC Vane

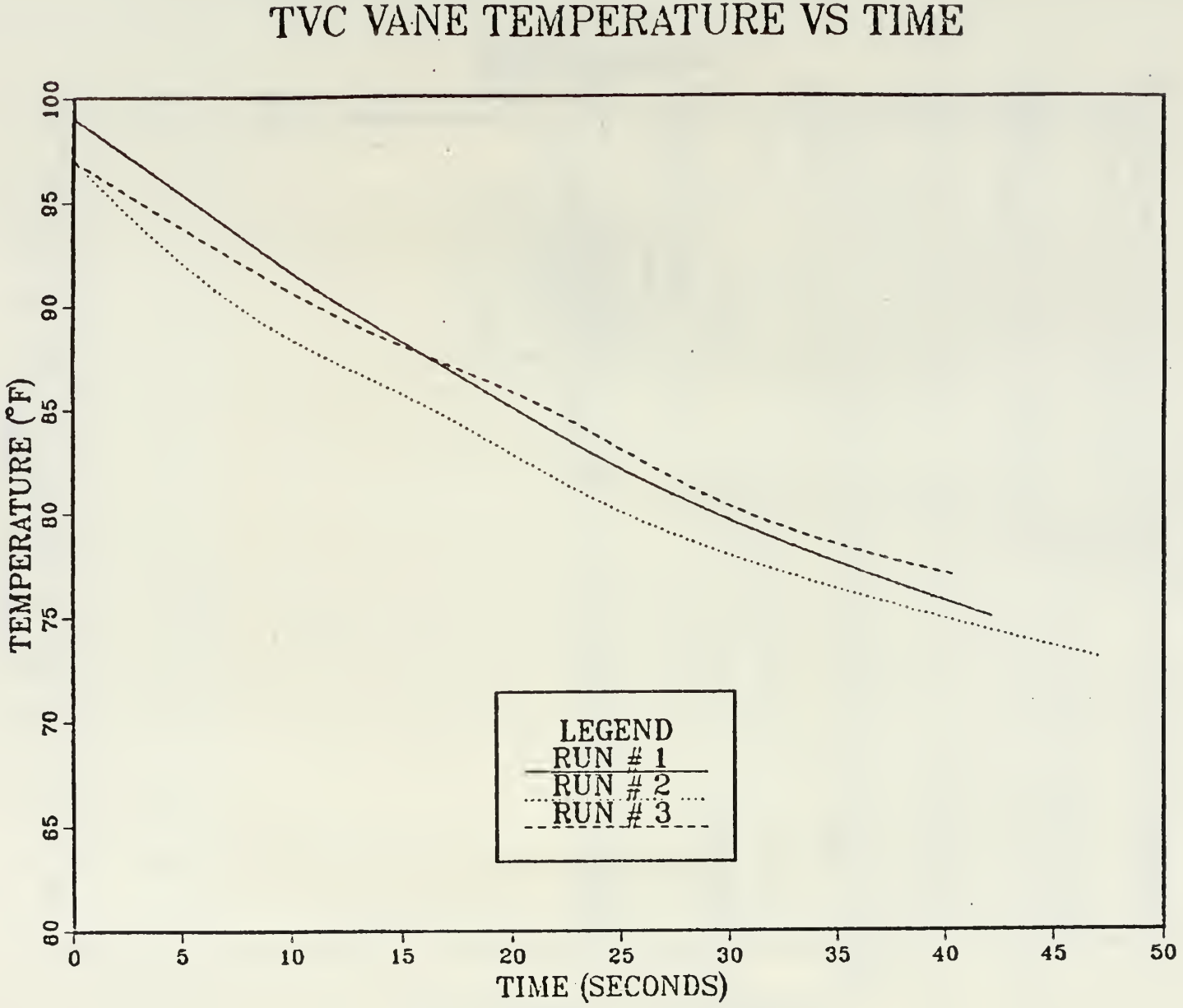

Figure 10. Graph of TVC Vane Temperature vs Time

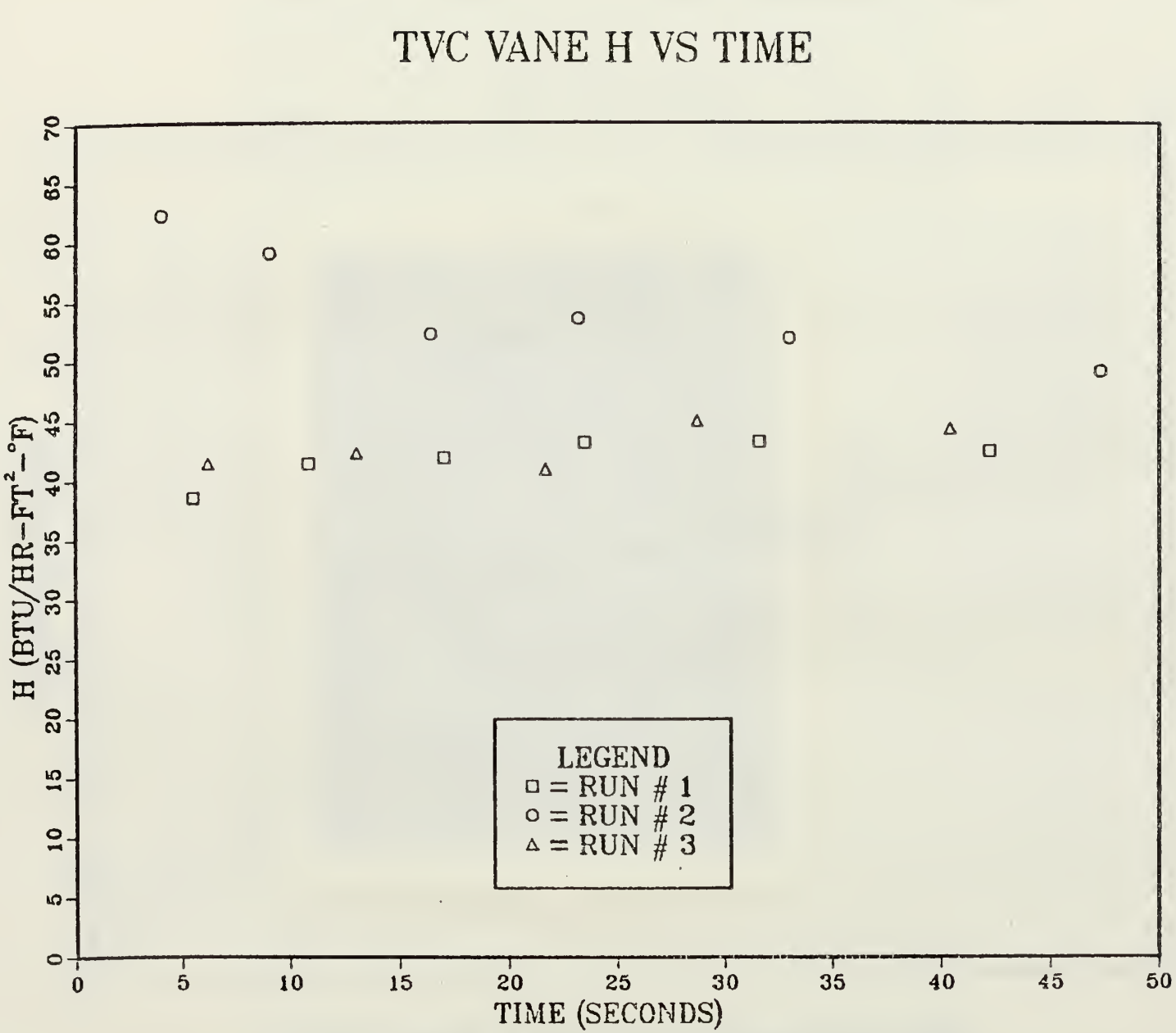

Figure 11. Graph of TVC Vane h vs Time

LIST OF REFERENCES

1. Holman, J.P., Heat Transfer, Third Edition, Chapter 4, McGraw-Hill Book Company, 1972.

2. Hughes Aircraft Company, PROBEYE Thermal Video System Series 4000 Operating Manual, Industrial Products Division, September, 1983.

3. Eastman Kodak Company Publication U-72, Kodak IRTRAN Infrared Optical Materials, Kodak Apparatus Division, 1981.

4. Department of Mechanical Engineering Memorandum NC4(69Xk), Flow Quality in Department of Mechanical Engineering Wind Tunnel in Building 500, by P. Ligrani, September 1985.

5. Software Arts, Inc., TK! SOLVER, Wellesley, Ma, 1982.

6. Incropera, Frank P., and David D. Dewitt, Fundamentals of Heat Transfer, Chapter 7.2, pp. 325-330, John Wiley and Sons, 1981.

7. Bolz, Ray E., and George L. Tuve, Handbook of Tables for Applied Engineering Science, Chemical Rubber Company Press, 1983.

INITIAL DISTRIBUTION LIST

		No. Copies
1.	Defense Technical Information Center Cameron Station Alexandria, VA 22304-6145	2
2.	Library, Code 0142 Naval Postgraduate School Monterey, California 93943-5002	2
3.	Department Chairman, Code 69 Department of Mechanical Engineering Naval Postgraduate School Monterey, California 93943-5000	2
4.	Professor Robert H. Nunn, Code 69Nn Department of Mechanical Engineering Naval Postgraduate School Monterey, California 93943-5000	3
5.	LCDR Timothy M. Spence 2409 Torrejon Place Carlsbad, California 92008	1

217584

Thesis
S66777 Spence
c.1 Applications of infrared thermography in convective heat transfer.